Radio Science, Volume 27, Number 1, Pages 31–46, January–February 1992

Excitation of whistler mode signals via injection of polarized VLF waves with the Siple transmitter

T. A. Mielke, C. J. Elkins, R. A. Helliwell, and U. S. Inan

Space, Telecommunications, and Radioscience Laboratory, Stanford University, Stanford, California

(Received September 4, 1990; revised July 2, 1991; accepted September 17, 1991.)

Whistler mode waves of various polarizations were transmitted by the Siple Station, Antarctica, VLF transmitter and received near the geomagnetic conjugate point at Lake Mistissini, Quebec. Crossed 21-km horizontal dipole antennas on top of the 2-km-thick ice sheet were used to transmit 2- to 4-kHz waves alternately with right-hand circular, left-hand circular, and linear polarizations. Excitation of a multiplicity of magnetospheric propagation paths and the received signal strength were observed to depend on the transmitter antenna polarization. Where whistler mode growth and emission triggering occurred, saturated peak values of received signals were independent of antenna polarization and initial injected power levels, in agreement with previous findings. Propagation paths of ducted Siple signals observed at Lake Mistissini were identified with propagation paths deduced from natural whistlers, from which the L shell values and equatorial number densities for the paths were calculated. A combination of L shell data and models of antenna coupling into the whistler mode may aid in the location of ducts. Dynamics Explorer 1 satellite recordings of unducted Siple signals showed trends similar to the ground data on ducted signals. The observations are discussed in the context of a simplified model of the coupling from the Siple antenna into the ionosphere, which provides reasonable agreement with observations.

INTRODUCTION

Magnetoionic theory as applied in a homogeneous medium with a vertical magnetic field and a sharp lower boundary predicts that an upgoing right-hand circular polarized wave normally incident to the lower ionosphere would couple twice as much power into the whistler mode as a linear polarized wave of the same strength and that a left-hand circular polarized wave would fail altogether at coupling into the whistler mode [*Budden*, 1985]. Thus only right-hand whistler mode waves are expected to be launched into the ionosphere, regardless of antenna polarization. This is a fair approximation of coupling into an overhead duct from an antenna on the ground in polar regions. Experiments made at Siple Station, Antarctica, at Lake Mistissini, Quebec, and on the Dynamics Explorer 1 (DE 1) satellite in 1986 displayed the expected hierarchy. A simple model of the coupling from a horizontal dipole antenna into the ionosphere and to variously positioned ducts can, in conjunction with observed multipath and magnetospheric wave growth, account for the observed data.

Paper number 91RS02457.
0048-6604/92/91RS-02457$08.00

DESCRIPTION OF THE EXPERIMENT

Siple station, Antarctica (76°S, 84°W) rests atop some 2 km of ice. This permits large horizontal half wave dipole antennas on the surface to operate with ≈1–3% efficiency [*Raghuram et al.*, 1974]. At the time of the experiments described, two 21-km crossed dipoles (see Figure 1) were in use. These antennas were laid out in the magnetic north-south and magnetic east-west directions. Six antenna polarizations were used: right-hand circular (abbreviated RH), left-hand circular (abbreviated LH), linear along a northeast-southwest axis (abbreviated D1), linear along a northwest-southeast axis (abbreviated D2), linear along a north-south axis (abbreviated NS), and linear along a east-west axis (abbreviated EW). Transmissions were made from Siple Station, with receivers at Lake Mistissini, Quebec, near the geomagnetic conjugate point and on the Dynamics Explorer 1 (DE 1) satellite. Various sequences (designated POLAD, POLA1, and POLA2) of constant-frequency pulses, interspersed with pulses of linearly varying frequency, were sent. Further details of the transmitter-receiver configurations can be found elsewhere [*Helliwell*, 1988].

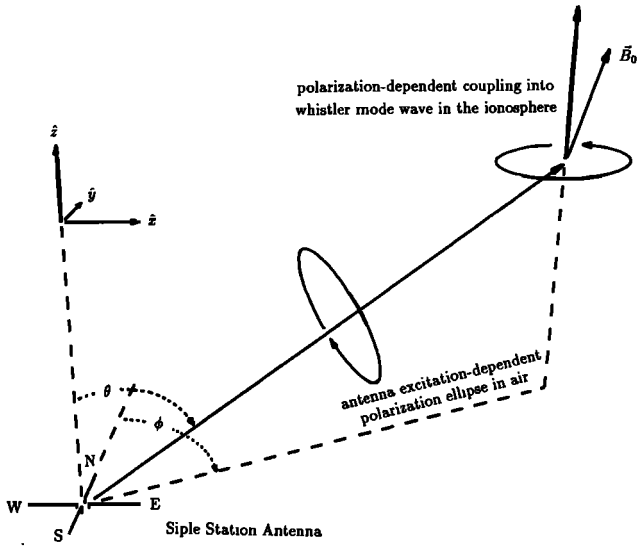

Fig. 1. Siple antenna layout.

ANTENNA COUPLING TO THE WHISTLER MODE

The Siple Station antenna layout is sketched in Figure 1. Radiation at frequencies from 2 to 12 kHz is incident on the ionosphere at a height of 70–90 km and generates whistler mode waves in the magnetosphere. The dependence of the whistler mode excitation on azimuth ϕ, zenith angle θ, and antenna polarization is developed here. Numerous approximations are employed in order to obtain closed-form expressions. The major assumptions are listed below.

1. The ionosphere is treated as an abrupt boundary, a common assumption in VLF problems [*Budden*, 1985]. This is justified by the large free-space wavelengths (of the order of 25–150 km) and the sharp boundary of the lower ionosphere (density changes from 10^{-2} to 10^{+1} cm^{-3} within <10 km) [*Inan et al.*, 1988].

2. At any given patch of ionosphere the direct ray from the transmitter and the ray reflected from the ice surface are combined into a single ray with constant phase and amplitude, independent of zenith angle θ. Polarization of this composite ray is that of the direct ray from the transmitter. Given the measured permittivity of Antarctic ice [*Peden et al.*, 1972], the reflection at the ice surface is nearly independent of both incidence angle and polarization up to a zenith angle of ≈60°. As the antenna is typically 2–3 m (less than 0.1% of a wavelength) above the surface of the ice, the path length difference between the direct ray and ice reflection is negligible.

3. Above 6 kHz the reflection from the rock beneath the ice is ignored. This ray must typically travel through several skin depths of ice and so is much weaker than the combination of direct ray and ice reflection. Below 6 kHz the ice attenuation is weaker, but due to the large relative permittivity of the ice sheet ($\varepsilon_r = 25 + j36$ at 4 kHz for example) the ray in the ice is nearly vertical regardless of incidence angle at the air-ice boundary. Thus the phase of the ray reflecting from the rock is nearly independent of zenith angle (in air), and this ray can be combined with the direct ray and ice reflection to produce a composite ray with phase and amplitude independent of zenith angle.

4. As observations are taken at great distances from Siple Station, near-field antenna terms are ignored. This is clearly the case for both Lake Mistissini ground data and DE 1 high-altitude satellite data.

With a slab model of the ionosphere and assumed incident plane waves the transmission coefficients for the excitation of whistler mode waves by parallel and perpendicular incident waves can be calculated. This is illustrated in Figure 2, with the transmission coefficients for $n \gg 1$ and $\theta < 60°$ derived from *Budden* [1961]. The Earth's magnetic field at Siple Station ($\mathbf{B}_0$) is 16.2° from the vertical, directed upward. This value was used in Budden's approximate formulas. After much algebra the incident parallel and perpendicular waves can be expressed in terms of the antenna excitations. Because of the ice and rock reflections discussed above, the effective antenna excitations (current on an ideal dipole in free space to obtain the same radiated power) are estimated to be about 25% of the actual antenna current. The resulting theory of coupling from antenna to whistler mode describes the essential physics of the process. High accuracy should not be expected from so simple a model, but the trends it predicts should be reliable. A list of definitions follows.

$\mathbf{E}^I$ incident wave on air-ionosphere boundary;
$E_\parallel^a$ transmitted wave in ionosphere (RH circular polarization, propagating);
$E_\parallel^b$ transmitted wave in ionosphere (LH circular polarization, evanescent);
$\mathscr{E}_A$ N-S antenna excitation, equal to $|\mathscr{E}_A|e^{i\delta_A}$;
$\mathscr{E}_B$ E-W antenna excitation, equal to $|\mathscr{E}_B|e^{i\delta_B}$;
F_A N-S antenna pattern;
F_B E-W antenna pattern;
$\hat{E}_A$ N-S antenna field unit vector;
$\hat{E}_B$ E-W antenna field unit vector;

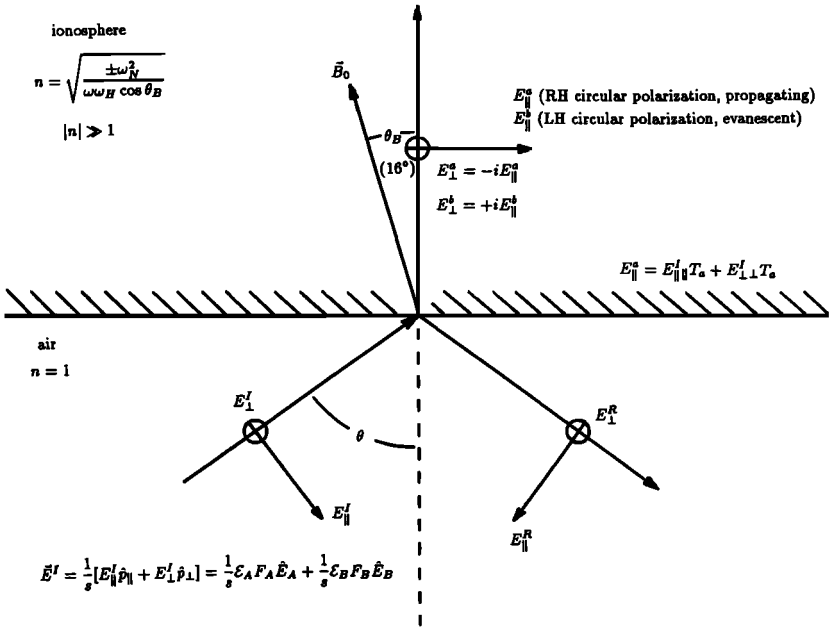

Fig. 2. Whistler mode excitation at the air-ionosphere boundary.

$\hat{p}_\parallel$ parallel field unit vector;
$\hat{p}_\perp$ perpendicular field unit vector;
s slant distance to antenna;
$_\parallel T_a$ $\parallel$ to RH transmission coefficient equal to $1/|n|$;
$_\perp T_a$ $\perp$ to RH transmission coefficient equal to $i \cos\theta/|n|$;
n refractive index in ionosphere equal to $[(\pm\omega_N^2)/(\omega\omega_H \cos\theta_B)]^{1/2}$;
n_a ordinary wave (whistler mode) refractive index equal to $|n|$;
n_b extraordinary wave refractive index equal to $-i|n|$;
δ_A NS antenna phase;
δ_B EW antenna phase;
L antenna length;
h ionosphere height;
p^a whistler mode power equal to $n_a|E_\parallel^a|^2$.

Using these definitions, the general case is

$$P^a = \frac{\cos^4\theta}{|n|h^2} \cdot \left[+|\mathcal{E}_A|^2 \left(\frac{\cos\langle(\pi L/\lambda)\sin\theta\cos\phi\rangle - \cos\langle\pi L/\lambda\rangle}{1-\sin^2\theta\cos^2\phi} \right)^2 + |\mathcal{E}_B|^2 \left(\frac{\cos\langle(\pi L/\lambda)\sin\theta\sin\phi\rangle - \cos\langle\pi L/\lambda\rangle}{1-\sin^2\theta\sin^2\phi} \right)^2 + 2|\mathcal{E}_A||\mathcal{E}_B| \left(\frac{\cos\langle(\pi L/\lambda)\sin\theta\cos\phi\rangle - \cos\langle\pi L/\lambda\rangle}{1-\sin^2\theta\cos^2\phi} \right) \cdot \left(\frac{\cos\langle(\pi L/\lambda)\sin\theta\sin\phi\rangle - \cos\langle\pi L/\lambda\rangle}{1-\sin^2\theta\sin^2\phi} \right) \cdot \sin(\delta_B - \delta_A) \right]$$

Two interesting special cases are $L \ll \lambda$ (short dipole)

$$P^a = \frac{\cos^4\theta}{|n|h^2}[|\mathcal{E}_A|^2 + |\mathcal{E}_B|^2 + 2|\mathcal{E}_A||\mathcal{E}_B|\sin(\delta_B - \delta_A)]$$

and $L = \lambda/2$ (half wave dipole)

$$P^a = \frac{\cos^4\theta}{|n|h^2} \left[+|\mathcal{E}_A|^2 \left(\frac{\cos\langle(\pi/2)\sin\theta\cos\phi\rangle}{1-\sin^2\theta\cos^2\phi} \right)^2 + |\mathcal{E}_B|^2 \left(\frac{\cos\langle(\pi/2)\sin\theta\sin\phi\rangle}{1-\sin^2\theta\sin^2\phi} \right)^2 + 2|\mathcal{E}_A||\mathcal{E}_B| \frac{\cos\langle(\pi/2)\sin\theta\cos\phi\rangle}{1-\sin^2\theta\cos^2\phi} \cdot \frac{\cos\langle(\pi/2)\sin\theta\sin\phi\rangle}{1-\sin^2\theta\sin^2\phi} \sin(\delta_B - \delta_A) \right]$$

The following antenna excitation values correspond to the experimental polarizations used at Siple Station:

RH	$\lvert\mathscr{E}_A\rvert = \lvert\mathscr{E}_B\rvert$	$\delta_B - \delta_A = \pi/2$
LH	$\lvert\mathscr{E}_A\rvert = \lvert\mathscr{E}_B\rvert$	$\delta_B - \delta_A = -\pi/2$
D1	$\lvert\mathscr{E}_A\rvert = \lvert\mathscr{E}_B\rvert$	$\delta_B - \delta_A = 0$
D2	$\lvert\mathscr{E}_A\rvert = \lvert\mathscr{E}_B\rvert$	$\delta_B - \delta_A = \pi$
NS	$\lvert\mathscr{E}_B\rvert = 0$	
EW	$\lvert\mathscr{E}_A\rvert = 0$	

At the zenith, both half wave and short crossed-dipole antennas give the same results. The major difference between results occurs for the LH transmitter polarization. In that case the half wave dipole antenna will excite the whistler mode off the zenith and away from the azimuth angles of 45°, 135°, 225°, and 315° (which form symmetry axes when both antennas are equally excited), while the short dipole antenna with LH polarization does not excite the whistler mode at any azimuth. Plots of the whistler mode power (coupled into the base of the ionosphere from the half wave crossed-dipole antenna) as a function of azimuth and distance from Siple Station are shown in Figure 3.

The determination of the ionospheric entry or exit points of a ducted whistler mode signal is difficult and is only discussed in general terms in one of the cases studied. Uncertain ionospheric absorption and propagation losses make absolute signal strengths difficult to obtain. In this paper, ratios of received signal strengths for different given transmitting antenna polarizations constitute the available experimental data. Because of the nulls in whistler mode excitation for LH antenna polarization, the ratios involving LH are sensitive to duct location relative to the antenna. Ratios of the power coupled into the whistler mode wave for various antenna polarizations do not change significantly between the short and half wave dipoles. RH/D (D1 and D2 give identical power ratios) has at maximum a 1% deviation from the short dipole result, while NS/RH and NS/D show a maximum of 20% deviation. This corresponds to 1 dB or less, which is below the natural fluctuations in received signal intensity. LH/RH, LH/D, and LH/NS increase from zero with the short dipole to 0.008, 0.015, and 0.04, respectively, for the half wave dipole. While the LH ratios show large percentage changes, the absolute changes remain small. Given the approximate nature of this model, the short dipole model is adequate for all but left-hand antenna polarization. In the case of left-hand antenna polarization the half wave model shows that some whistler mode waves can be excited but probably underestimates the strength of the excitation. Factors ignored in this model, such as ice reflections, rock reflections, near-field effects, mode conversion in the ionosphere, etc., can all be expected to degrade the purity of the left-hand transmission and therefore increase the coupling into the whistler mode wave.

OBSERVATIONS OF DUCTED SIGNALS WITH DISCRETE PATHS IDENTIFIABLE

Figure 4 displays spectrograms showing 1 kHz/s frequency ramps transmitted at Siple Station and received at the conjugate station, Lake Mistissini. Four time periods are shown, two during May 29, 1986, and two during May 30, 1986. These spectrograms illustrate the predicted power relationships between differently polarized transmissions, RH > D2 ≈ D1 > LH. The physical picture behind these power relationships is straightforward. The polarization ellipse of a plane wave from the antenna, when projected on the air-ionosphere boundary, will generally contain a component of RH circular polarization. It is this RH circular element which couples into the whistler mode. The RH circular component is maximum for a RH circular antenna polarization and minimum for a LH circular antenna polarization. Linear antenna polarizations D1 and D2 are intermediate cases. Note the repeatability throughout an hour and from day to day. The amplitudes given for each polarization represent the peak value of the strongest ramp at 3.477 kHz for May 29 and 3.96 kHz for May 30. A 100-Hz filter bandwidth was used in this measurement. These values should only be taken as a rough measure of the relative intensities between polarizations. Although D2 has the same peak value as RH for its strongest ramp, RH shows the strongest response and excites the largest number of paths. LH shows the weakest response and excites the fewest number of paths.

Modeling of coupling from the antenna into the ionosphere indicates that for fixed transmitter power, power ratios between different transmitter polarizations change with zenith angle and azimuth. If we know the location of the field-aligned ducts that the signals travel in, we can determine zenith angle θ and azimuth ϕ, then predict the power ratios that we should see between antenna polarizations. This provides a method for testing the model.

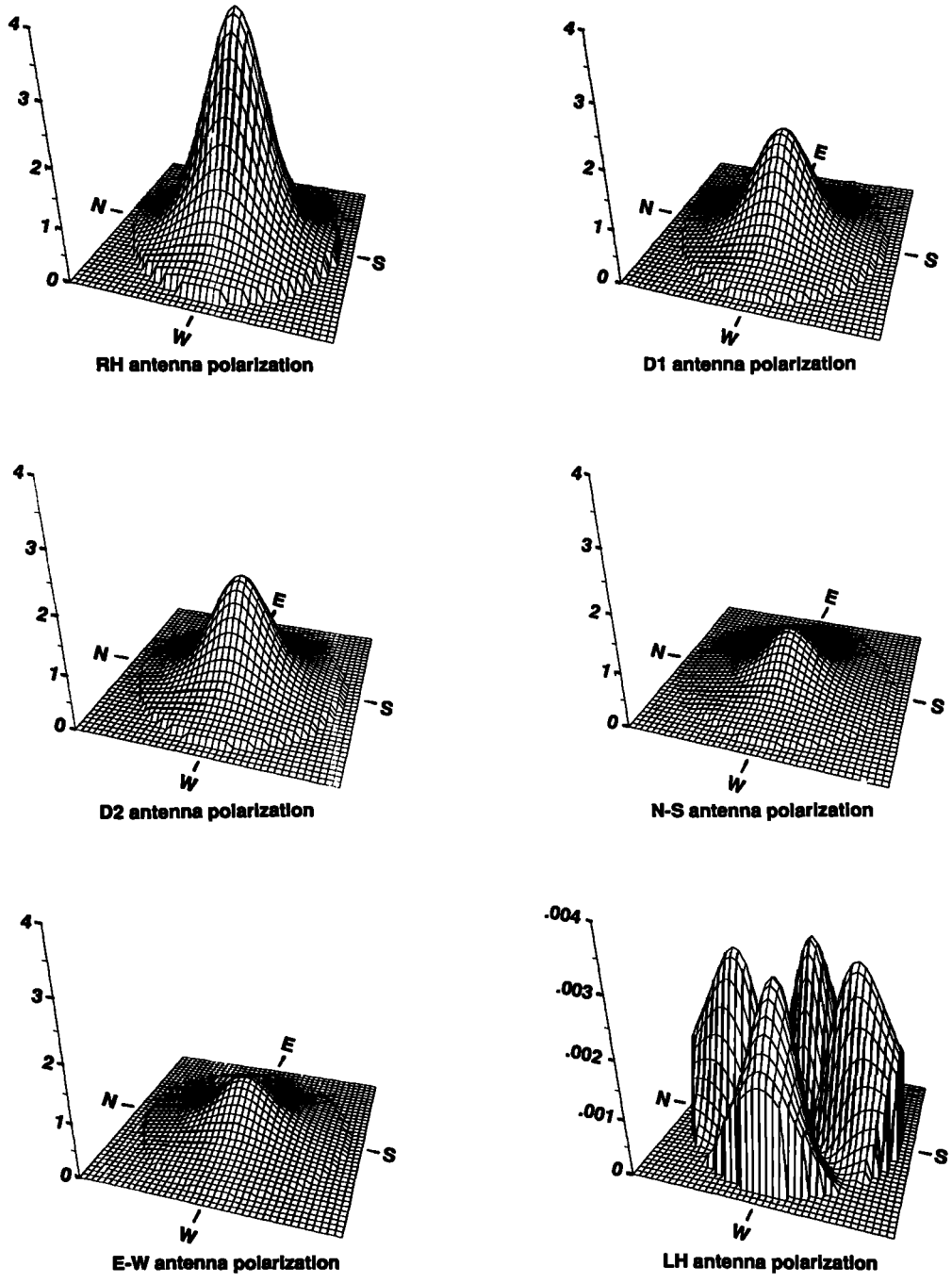

Fig. 3. Plots of power coupled into the whistler mode wave at the air-ionosphere boundary (relative to the power coupled at the zenith from a single antenna) for various antenna polarizations. All plots are centered on Siple Station. Plots end at a zenith angle of 60° (corresponding to a 155-km radius for an ionospheric height of 90 km). Antennas are half wave dipoles. Note that coupling from LH antenna polarization is much weaker than coupling from other antenna polarizations and also exhibits distinct nulls.

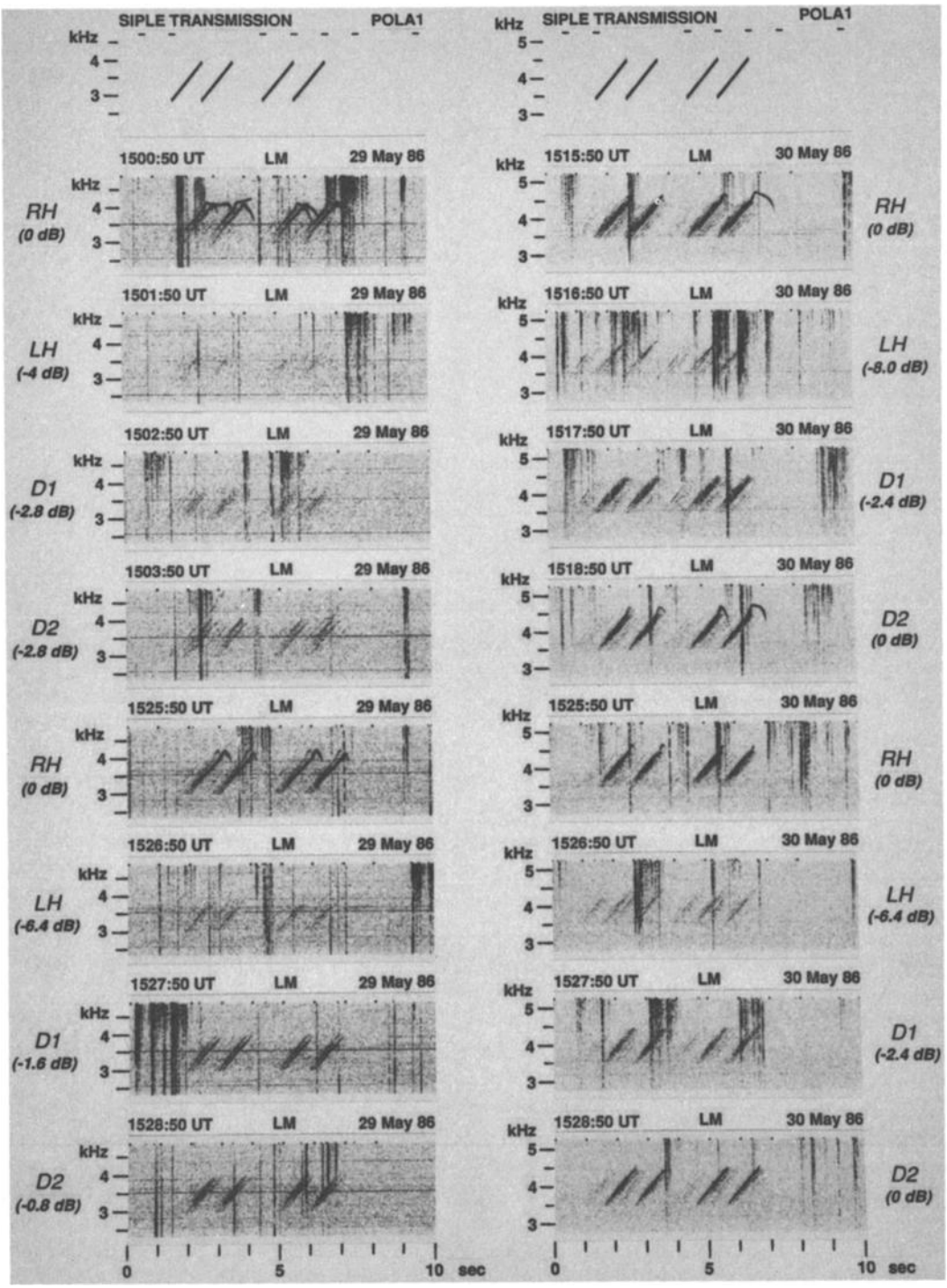

Fig. 4. Polarization experiments with transmitted frequency ramps. Peak power at center frequency is shown in parentheses for various antenna polarizations.

However, we also need to consider attenuation from Siple to the duct entry point in the south and from the duct exit point in the north to Lake Mistissini. The procedure used to determine the location of the ducts was (1) to determine the time delay of each 1 kHz/s ramp at a specific frequency (2.7 kHz in this case), (2) to compare this to the whistlers and their time delays at the same frequency and then, by finding a whistler with the same time delay, to identify the whistler corresponding to the specific path taken by the ramp, (3) to determine the nose frequency and nose time delay for this whistler and calculate the L shell and equatorial electron density of the associated path [*Ho and Bernard*, 1973], and (4) once the L shell is known, to map it relative to Siple Station and to estimate the zenith angle and azimuth of the path end point. (Unless the L shell indicates otherwise, the duct entrance point is assumed to be within 100 km of Siple Station [*Carpenter*, 1980].)

An example of this procedure is illustrated in Figures 5, 6, and 7. Figure 5 displays a spectrogram showing the transmitted signal (1 kHz/s frequency ramp) along with a spectrogram and a chart of the amplitude in a 300-Hz band centered at 2.7 kHz for the signal received at Lake Mistissini. Due to multipath effects each signal transmitted at Siple Station gives rise to five signals at Lake Mistissini, designated P1–P5. A spectrogram of a multipath whistler and its sferic as observed at Siple shortly after this transmission is also shown. The whistlers labeled WP1–WP5 have delay times corresponding to ramps P1–P5. L shells and equatorial electron densities for these whistlers are indicated. It is necessary to obtain L shells from the whistlers rather than from the frequency ramps due to the difficulty of making good dispersion measurements on the much narrower band frequency ramps. Note that the path WP1 has a much smaller equatorial number density than any of the other whistler paths. This is presumably due to longitudinal variations in the L value of the plasmapause. Such effects have been seen in previous whistler studies [*Angerami and Carpenter*, 1966].

In Figure 6, spectrograms showing the Siple transmitted signal, RH- and LH-polarized signals as received at Lake Mistissini, and charts of received amplitude in a 100-Hz band centered at 2.7 kHz are shown. For the RH-polarized transmission, four paths labeled 6P1–6P4 are evident at Lake Mistissini. Paths 6P1, 6P3, and 6P4, correspond to paths P1, P2, and P5, respectively, of Figure 5. No whistler corresponding to path 6P2 was found. For the LH-polarized transmission, only paths 6P1 and 6P4 can be seen at Lake Mistissini. As all paths show evidence of growth and triggered emissions, and since the saturated power of a signal after magnetospheric growth is not dependent on input signal power [*Helliwell et al.*, 1980], it is no surprise to see that the LH and RH powers received on paths 6P1 and 6P4 are similar. The magnetospheric growth which can be observed in this experiment corresponds to the "temporal growth" of [*Helliwell et al.*, 1980] or the "nonlinear amplification" of [*Dowden et al.*, 1978]. This magnetospheric growth exhibits a threshold effect, in which weak input signals produce no growth, but stronger input signals result in growth to the saturated power level [*Helliwell et al.*, 1980]. Thus on paths 6P2 and 6P3 the RH transmission was presumably above the threshold for growth, while the LH transmission was not. As sketched in Figure 7, path 6P3 is on the 4.53 L shell and is probably nearest to the symmetry axes at 45° to the antenna, where the LH polarized transmission coupling to the ionosphere approaches zero. Paths 6P1 and 6P4 are on L shells of 4.62 and 4.53, respectively, away from the LH nulls and within 100 km of Siple Station.

OBSERVATIONS OF DUCTED SIGNALS WITH MULTIPATH EFFECTS PRESENT

Multipath effects are also present on single frequency signals most of the time. One result of multipath is that the received pulse is longer than the transmitted pulse and the received amplitude is the sum of several pulses with different amplitudes, time delays, and magnetospheric growth histories. Rarely can these components be disentangled. However, if the multipath effects are severe, with numerous paths contributing to the received signal, an estimate of the impact can be made as follows. Assume that the received signal is dominated by those paths on which the whistler mode input signal is above the threshold for growth. On average, these paths will each produce similar saturated powers that combine in an incoherent manner at the receiver. If the ducts that give rise to these paths are both numerous and distributed more or less uniformly in the ionosphere above the transmitter, the number of ducts above threshold will depend on the ionospheric area in which strong coupling from

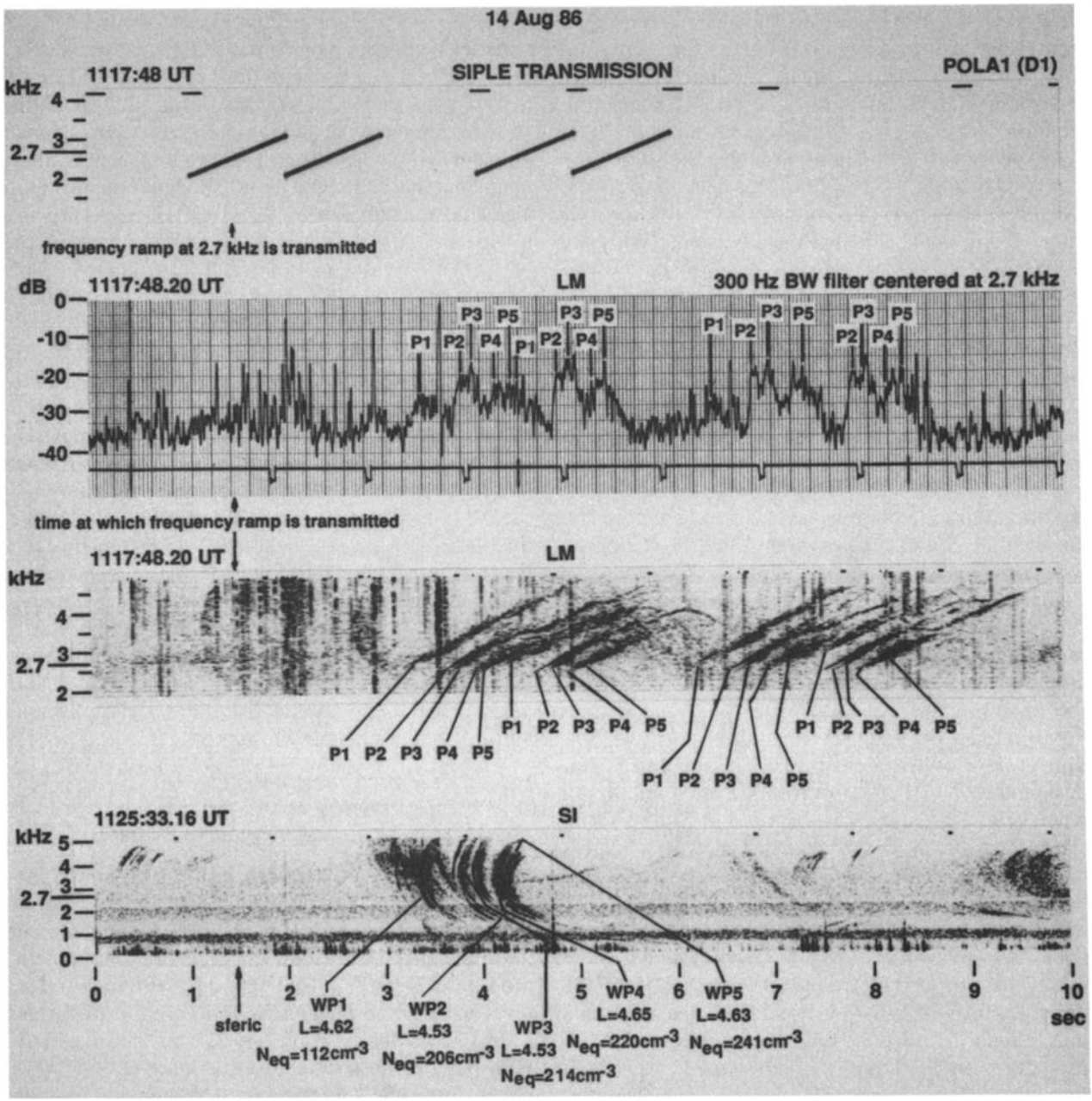

Fig. 5. Propagation path observations for Siple signals and whistlers with identical time delays.

the antenna to the whistler mode is present. The ratio of powers received from different transmitter polarizations of single-frequency pulses thus depends on the areas that these polarizations illuminate above the threshold for growth rather than on the ratios of whistler mode coupling at any particular duct. Unlike the single path cases of Figure 6 (where saturation effects can cause near equality of received signals with different transmitter polarizations despite lower magnetospheric input for one of them) this process preserves the hierarchy RH > D2 ≈ D1 > LH (since, given a fixed threshold for growth, these transmitter polarizations excite, respectively, smaller ionospheric areas above that threshold).

Figure 8 shows an example of this multipath

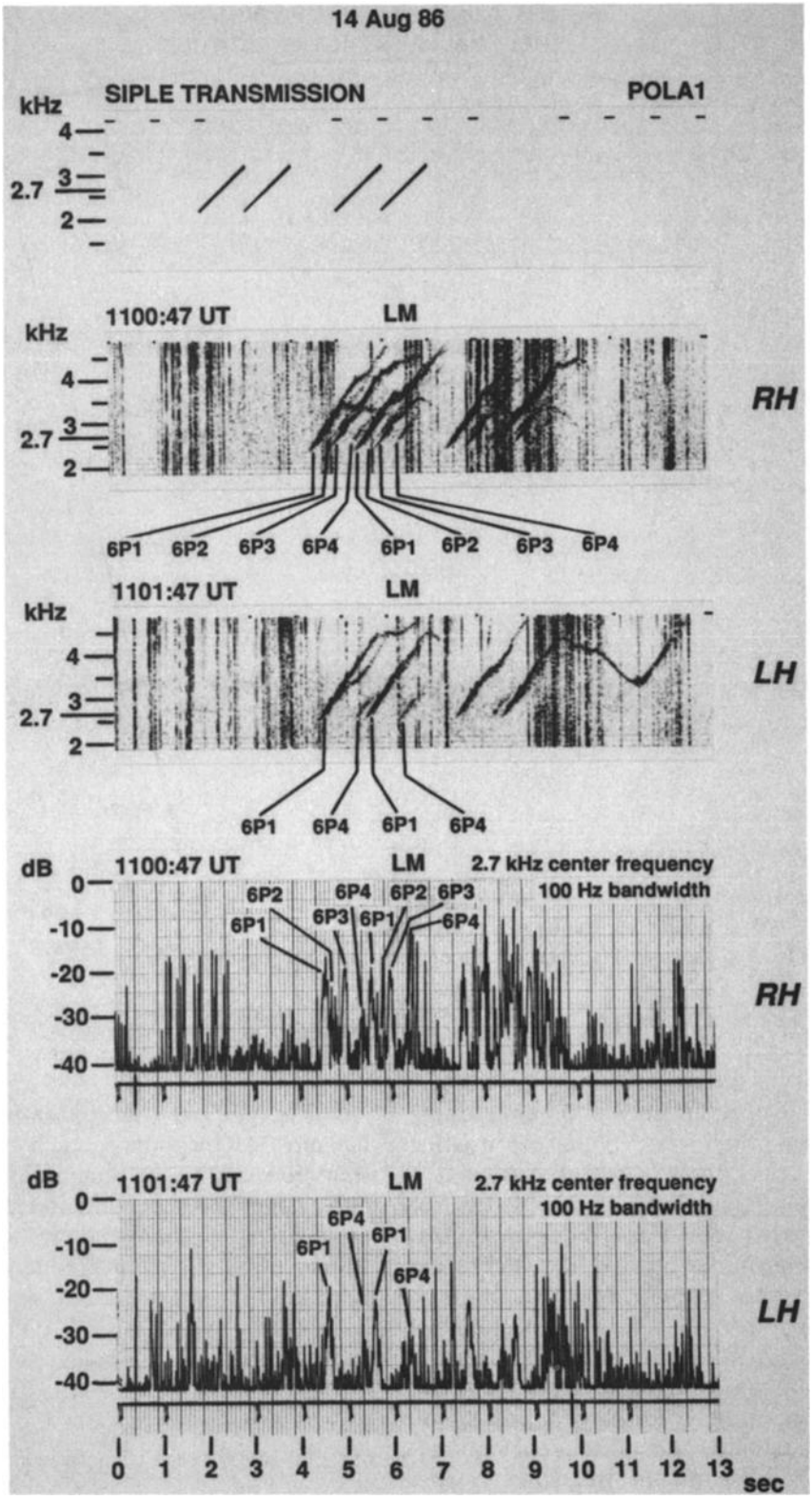

Fig. 6. Path selectivity of polarized transmissions.

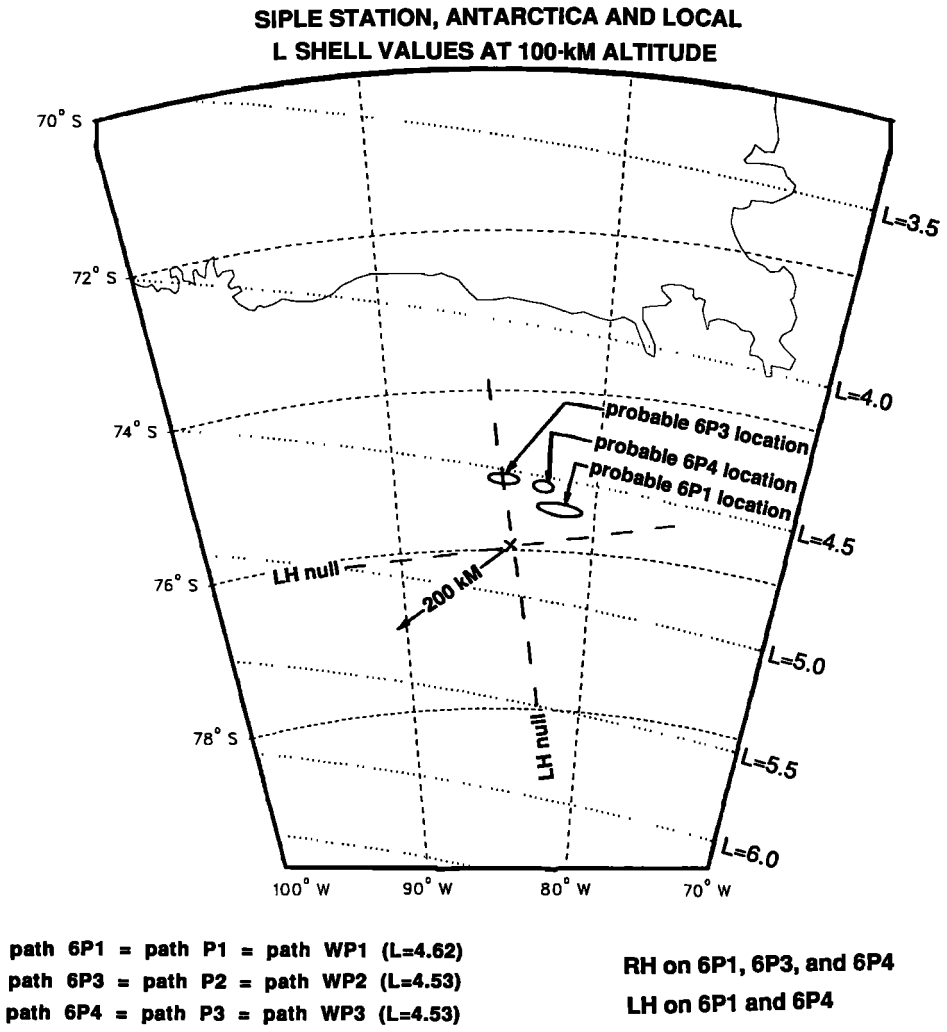

Fig. 7. Estimation of path endpoint location.

effect. The top spectrogram shows the Siple transmission to illustrate the format. A pulse consisting of a single frequency for 1 s followed by a 1 s doublet with 30-Hz separation is transmitted twice. This is followed by four 1 kHz/s frequency ramps, each 1 s long. Transmitter polarization is constant for the 22-s segments shown. Spectrograms and charts of amplitude in a 100-Hz band centered at 3.48 kHz are shown for RH and LH transmitter polarizations as received at Lake Mistissini. The peak RH amplitude is about 7.6 dB greater than the peak LH amplitude on the single-frequency pulses. The cause can be seen on the frequency ramps, where P′ labels a path excited only by RH transmissions and PG labels a group of paths excited by both RH and LH transmitter polarizations. Note that most of the ramps reach threshold, grow to saturation, and trigger emissions for the RH transmitter polarization, while fewer of the LH transmitter polarization ramps show emissions. In a like manner on the constant-frequency pulses the triggered emissions are more numerous and start nearer the leading edge on the RH transmitter polarization.

OBSERVATIONS OF DUCTED SIGNALS WITH SINGLE PATH PROPAGATION

Figure 9 shows a rare instance of single-path propagation for which magnetospheric growth and

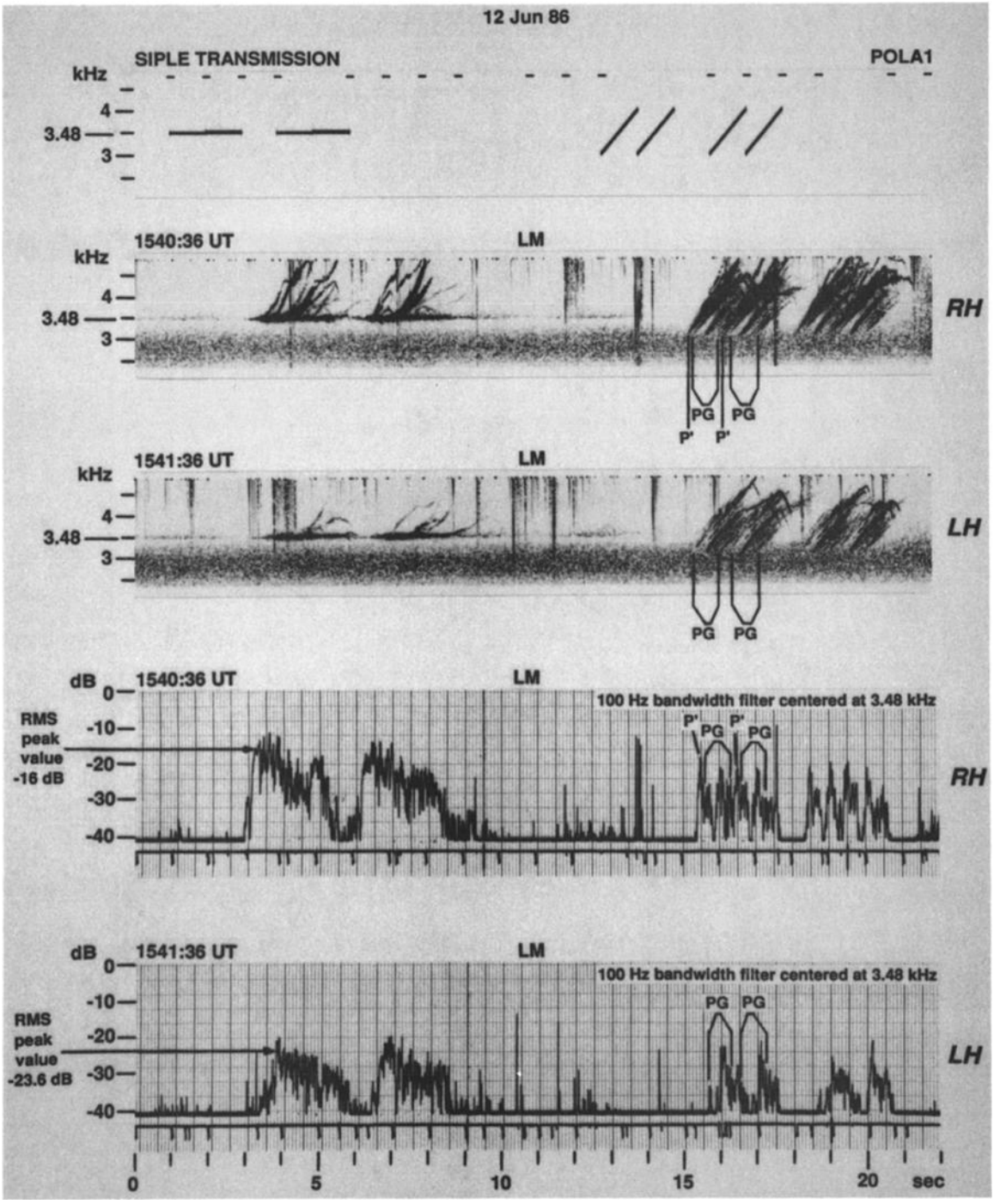

Fig. 8. Multipath ducted signals.

triggered emissions occurred. The transmitter format in this case is a single-frequency, amplitude-modulated pulse. For the first half second the amplitude increases at the rate of 20 dB/s, after which the amplitude remains constant for the remaining half second. Each successive pulse is of a different transmitter polarization. Spectrograms and charts of amplitude in a 300-Hz bandwidth,

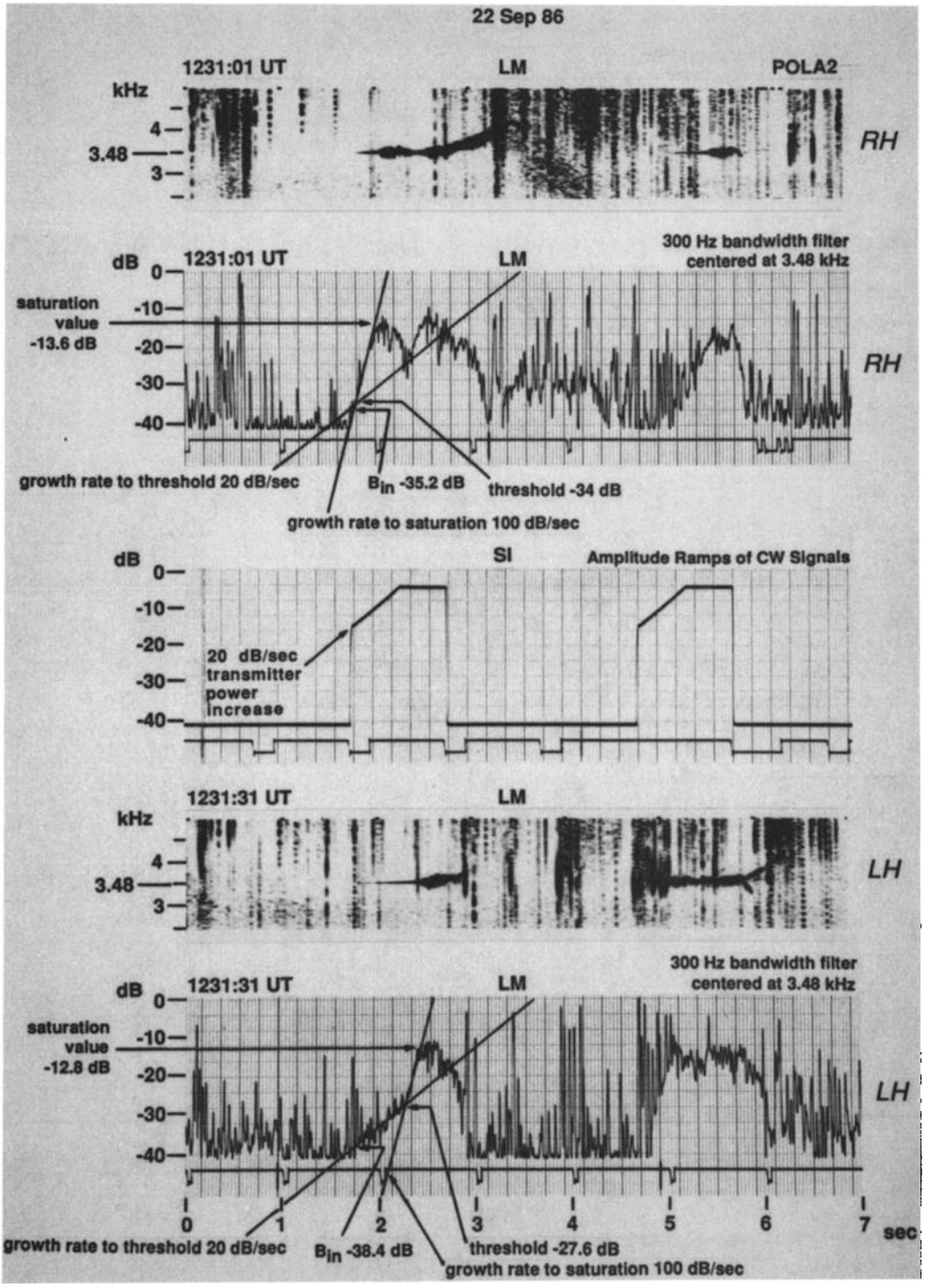

Fig. 9. Magnetospheric growth of Siple signals.

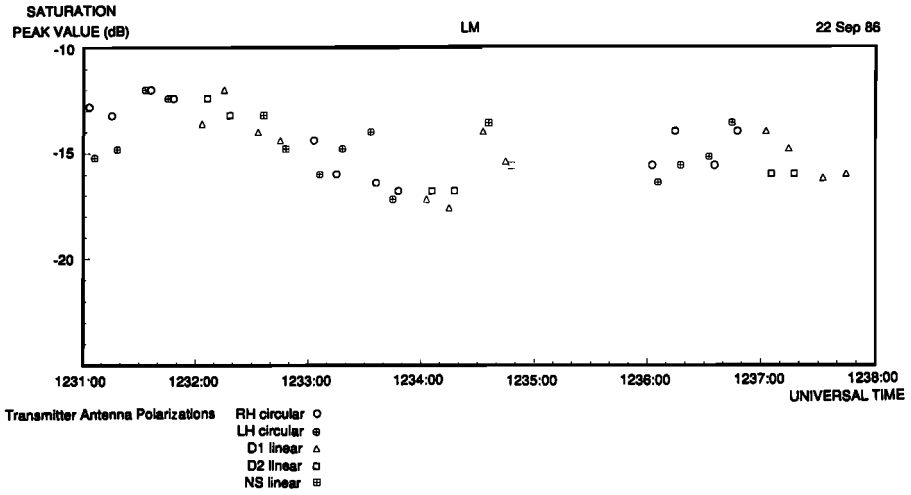

Fig. 10. Saturated power on single-path propagation.

centered at 3.48 kHz for the signal received at Lake Mistissini, are shown. An example of the transmitted signal is also provided. The pulse at 1231:03 UT was transmitted with RH polarization. Its initial amplitude was very close to the threshold for magnetospheric growth, so the signal's 20 dB/s amplitude ramp is seen for only 50 ms. At this time the signal strength crosses the threshold, and growth becomes independent of the signal input level; we see 100-dB/s growth, although the transmitted signal amplitude was increased at a rate of only 20 dB/s. Once the saturation level is reached, growth stops. Note that growth to saturation occurs twice and is also detectable on the spectrogram. A rising emission is triggered at pulse termination and continues for about 1 s.

The pulse at 1231:33 UT was transmitted with LH polarization. Note that the initial amplitude is 3.2 dB less than that of the RH transmitted signal. The growth rate to threshold is 20 dB/s for almost the entire 0.5 s. Once threshold is reached, though, the behavior is exactly that which is seen for RH; that is, 100-dB/s growth until saturation is reached. Even the saturation levels agree. The threshold values on these two pulses are not the same even though the consistent time delays and single-path propagation conditions of this data set indicate that they traveled in the same duct. The threshold level has been seen to change quickly with time [*Helliwell et al.*, 1980], and a 7-dB change in 30 s as seen here is not unreasonable. The threshold values between RH and LH transmitted signals only 3 s apart were measured at −34.4 dB (RH, 1231:03 UT) versus −32.4 dB (LH, 1231:06 UT) and −34.4 dB (RH, 1231:15 UT) versus −33.6 dB (LH, 1231:19 UT). Given the difficulties in measuring these levels in the presence of atmospheric noise, they agree fairly well.

Results of similar measurements made for the period of 1231–1238 UT on September 22, 1986, are shown in Figure 10. Although temporal variation in the saturation level is 3–4 dB, the average difference between RH and LH values is only 0.33 dB when the signals are measured close enough together in time (3 s) to minimize the effects of temporal variations.

OBSERVATIONS OF NONDUCTED SIGNALS

Examples of observations of polarized Siple transmissions on the DE-1 are shown in Figure 11. A 30-s segment consisting of a spectrogram of the Siple transmission (shifted by 2.5 s so as to line up with the satellite data), a spectrogram of the signal received on DE 1, and an amplitude from a 300-Hz-wide filter that was centered at 4.8 kHz demonstrates the increased coupling into the whistler mode of RH versus LH transmitter polarizations. Note that the presence of impulsive noise requires some care in determining amplitudes of the Siple signal. Also shown are spectrograms of frequency ramps observed on DE 1 at 0323:25 UT and 0329:25 UT with an example of the ramps transmitted at Siple Station. Both multipath and temporal fading

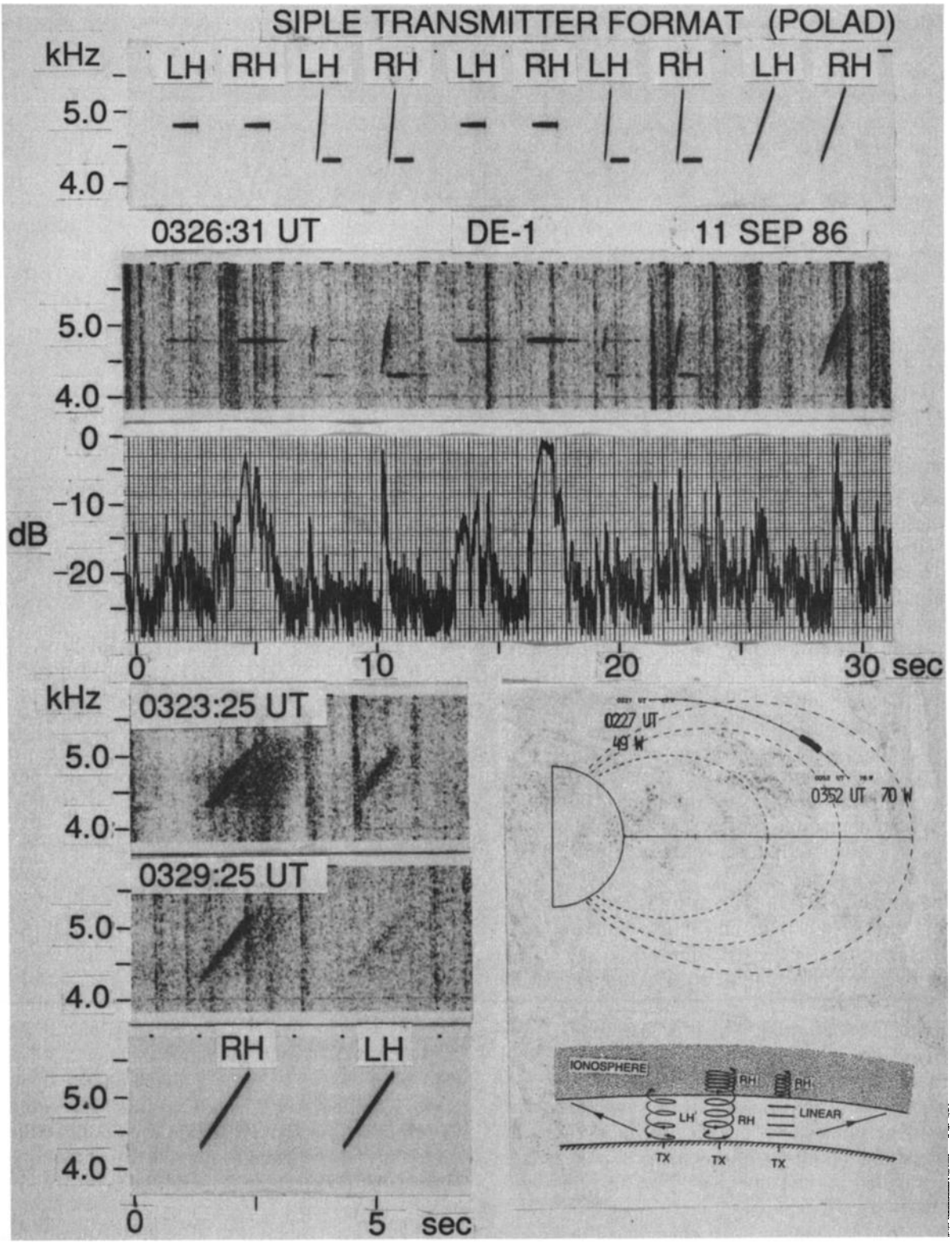

Fig. 11. Satellite observation of nonducted Siple signals.

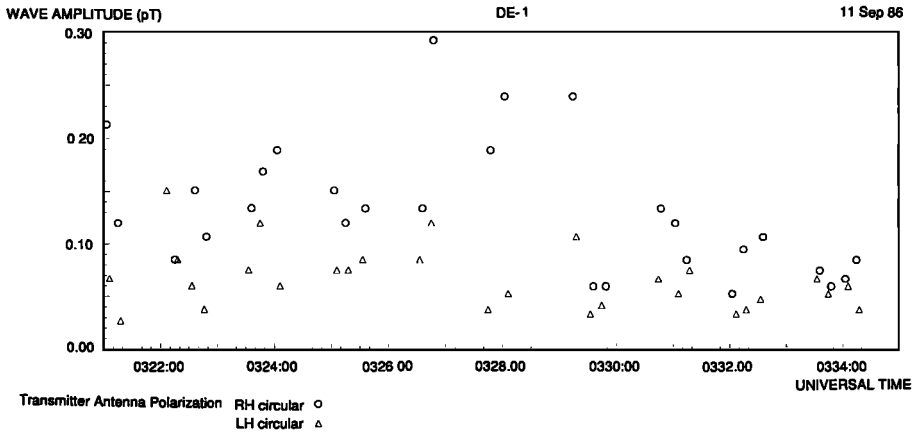

Fig. 12. Wave amplitude observed on DE 1 satellite from 112-kW Siple Station transmitter.

are apparent. A meridional plane projection of the DE 1 orbital position is also shown for reference. Measured wave amplitude (in picoteslas) of the Siple signal as seen on DE 1 as a function of time is shown in Figure 12. These data were obtained with the magnetic loop antenna coupled to the linear wave receiver [*Shawhan et al.*, 1981; *Sonwalker and Inan*, 1986]. A 300-Hz filter centered at 4.8 kHz was used to process the wideband satellite recordings. Data were also taken with the electric antenna, but reliable amplitudes could not be obtained due to spin fading (spin period of 6 s), causing gaps of up to a minute in the plotted results. At Siple Station the power input to the antennas was 62 kW for the E-W leg and 50 kW for the N-S leg. As there is no evidence of magnetospheric growth on this data set, the variations in signal intensity are presumably due to a combination of temporal variations in ionospheric coupling along with multiple ray paths reaching the satellite [*Sonwalkar et al.*, 1984]. The frequency ramps in Figure 11 show clear evidence of such multipath, and an orbit passing through regions of focusing and defocusing of ray paths should exhibit variations in signal intensity. Despite these complications, the RH transmitter polarization is always greater than or approximately equal to the LH transmitter polarization response. This agrees with the theory for whistler mode excitation in the absence of magnetospheric growth.

SUMMARY AND DISCUSSION

Experimental data from transmitter polarization experiments at Siple Station are in general agreement with predictions based on classic magnetoionic theory. More accurate modeling of the coupling from transmitter to whistler mode can, in conjunction with L shell information, identify likely duct locations. Such efforts would involve taking advantage of the lobed structure of the LH transmitter coupling while using dispersion to identify the L shell. Ionosonde and imaging riometer data would be required to produce a satisfactory model given the changeable nature of the ionosphere. The possibility of selectively exciting a single field-aligned duct is likewise of utility both for the study of the ducting process and in providing better data on the wave-particle interaction responsible for magnetospheric growth. Also, the whistler mode power available using RH transmitter polarization is about twice that available from linear polarization, as shown in Figure 3. This increased whistler mode power is of particular value in experiments aimed at artificial precipitation of energetic particles. The improved power achieved using RH polarization allows excitation of more paths above threshold, providing possible motivation for using a lower-power crossed-dipole antenna instead of a more powerful single-dipole antenna.

Acknowledgments. We thank John Katsufrakis for management of the field programs in which the data were acquired and Jim Logan for his service at Siple Station operating the transmitter. The contributions of Ev Paschal, Bill Trabucco, Tom Wolf, and Dave Shafer in designing, building, and installing the polarization controller at Siple Station and of Jerry Yarborough in data analysis are also greatly appreciated. This research was supported by National Science Foundation under grants DPP 86-13783 and DPP 89-18326.

REFERENCES

Angerami, J. J., and D. L. Carpenter, Whistler studies of the plasmapause in the magnetosphere, *J. Geophys. Res.*, *71*, 711–725, 1966.

Budden, K. G., *Radio Waves in the Ionosphere*, pp. 116–119, Cambridge University Press, New York, 1961.

Budden, K. G., *The Propagation of Radio Waves*, pp. 304–309, Cambridge University Press, New York, 1985.

Carpenter, D. L., Fast fluctuations in the arrival bearing of magnetospherically propagating signals from the Siple, Antarctica, VLF transmitter, *J. Geophys. Res.*, *85*, 4157–4166, 1980.

Dowden, R. L., A. D. McKay, L. E. S. Amon, H. C. Koons, and M. H. Dazey, Linear and nonlinear amplification in the magnetosphere during a 6.6-kHz transmission, *J. Geophys. Res.*, *83*, 169–181, 1978.

Helliwell, R. A., VLF wave simulation experiments in the magnetosphere from Siple Station, Antarctica, *Rev. Geophys.*, *26*, 551–578, 1988.

Helliwell, R. A., D. L. Carpenter, and T. R. Miller, Power threshold for growth of coherent VLF signals in the magnetosphere, *J. Geophys. Res.*, *85*, 3360–3366, 1980.

Ho, D., and L. C. Bernard, A fast method to determine the nose frequency and minimum group delay of a whistler when the causative spheric is unknown, *J. Atmos. Terr. Phys.*, *35*, 881–887, 1973.

Inan, U. S., W. C. Burgess, T. G. Wolf, and D. C. Shafer, Lightning-associated precipitation of MeV electrons from the inner radiation belt, *Geophys. Res. Lett.*, *15*, 172–175, 1988.

Peden, I. C., G. E. Webber, and A. S. Chandler, Complex permittivity of the Antarctic ice sheet in the VLF band, *Radio Sci.*, *7*, 645–650, 1972.

Raghuram, R., R. L. Smith, and T. F. Bell, VLF Antarctic antenna: Impedance and efficiency, *IEEE Trans. Antennas Propag.*, *AP-22*, 334–338, 1974.

Shawhan, S. D., D. A. Gurnett, D. L. Odem, R. A. Helliwell, and C. G. Park, The plasma wave and quasi-static electric field instrument (PWI) for Dynamics Explorer-A, *Space Sci. Instrum.*, *5*, 535–550, 1981.

Sonwalker, V. S., and U. S. Inan, Measurements of Siple transmitter signals on the DE 1 satellite: Wave normal direction and antenna effective length, *J. Geophys. Res.*, *91*, 154–164, 1986.

Sonwalker, V. S., T. F. Bell, R. A. Helliwell, and U. S. Inan, Direct multiple path magnetospheric propagation: A fundamental property of nonducted VLF waves, *J. Geophys. Res.*, *89*, 2823–2830, 1984.

C. J. Elkins, R. A. Helliwell, U.S. Inan, and T. A. Mielke, STAR Laboratory, Durand 325, Stanford University, Stanford, CA 94305.